Figure 13 shows the differences in ullage pressure observed on two recent S-II flights (AS-507 and 508). Figure 14 is an analog response run of the two flights using the previous ullage pressure curves. The system is excited by a small random noise input into the thrust. Complete time-varying coefficients were used in this simulation. The two cases show at least a qualitative explanation of the differences observed in the AS-507 and AS-508 flights. The large oscillation occurred on AS-508, shutting off the center engine near the same point where saturation occurs on the analog computer. Since the computer was not scaled to an amplitude large enough to duplicate flight, no direct comparison can be made.

Figure 15, showing the characteristics of the oscillations, is a blow-up of one of the computer runs in a nonlinear, unstable region. The LOX pump pressure has the same characteristics observed on flights, a short upper peak with a rounding or flattening on the bottom. Also, the harmonic is shown to be shifting downward as the AS-508 flight record showed.

Conclusions

The results to date show a qualitative explanation of some of the anomalies observed in Saturn Apollo POGO oscillations. The results are not at all quantitative and do not yet explain all the characteristics seen on these flights; for example, the decaying of oscillation in AS-504 near the end of burn after the oscillation had clearly reached the highly nonlinear range. The need for many sensitivity studies and care in making any changes in system parameters are strongly indicated, as well as the need for a better understanding of the physical phenomena and thus more accurate models. Particularly are the bubble characteristics and pump characteristics in need of additional theoretical and test analyses in order to substantiate the character of the assumed nonlinearity.

References

[1] Rubin, S., "Longitudinal Instability of Liquid Rockets Due to Propulsion Feedback (POGO)," *Journal of Spacecraft and Rockets*, Vol. 3, No. 8, Aug. 1966, pp. 1188–1195.

[2] Sack, L. E. and Nottage, H. B., "System Oscillations Associated with Cavitating Inducers," *Transactions of the ASME, Journal of Basic Engineering*, Vol. 87, Ser. D, No. 2, Dec. 1965, pp. 917–924.

[3] Stripling, L. B. and Acosta, A. J., "Cavitation in Turbopumps," *Transactions of the ASME, Journal of Basic Engineering*, Vol. 84, Ser. D, No. 3, Sept. 1962, pp. 339–350.

DECEMBER 1970 J. SPACECRAFT VOL. 7, NO. 12

Hypervelocity Impact of Bumper-Protected Fuel Tanks

PEI CHI CHOU* AND SHUN CHEN†

Drexel University, Philadelphia, Pa.

The problem of the fracture of bumper-protected, liquid-filled fuel tanks subjected to hypervelocity meteoroid impact is studied. The method of characteristics in finite difference form is applied to the equations governing stress wave propagation in the tank walls. The pressure field of the debris cloud from the perforated bumper is obtained from a semiempirical formula. The reaction of the liquid fuel due to the wall motion is calculated from the shock Hugoniot of the fuel and the wall velocity. Deflections calculated from the present theory are in good agreement with experimental measurements. The deflection and stress levels in a fuel tank are found to be one order of magnitude smaller than those produced in an empty tank.

Nomenclature

a,b = constants
c_p = plate velocity = $[E/\rho_1(1-\nu^2)]^{1/2}$
c_2 = shear wave velocity = $(G/\rho_1)^{1/2}$
D = flexural rigidity = $Eh^3/12(1-\nu^2)$
E = modulus of elasticity
G = shear modulus = $E/2(1+\nu)$
h = plate thickness
k_2 = shear correction factor
M_r,M_θ = radial and tangential bending moments, respectively
P = pressure loading function
P_1 = pressure constant
P_o = pressure ahead of shock front
P_f = pressure behind shock front
Q_r = transverse shear stress resultant
r = radial distance
t = time
t_1,t_o, = time constants
U = shock front velocity
u = particle velocity of liquid behind shock front
w = transverse displacement of the midplane
z = transverse distance from midplane
β = constant
ν = Poisson's ratio
ρ = density of liquid behind shock front
ρ_1 = density of plate
ρ_o = density of liquid ahead of shock front
σ_r,σ_θ = normal stresses due to M_r and M_θ, respectively
τ_{rz} = shear stress due to Q_r
ϕ = rotation of the cross section about the tangential axis‡

Presented as Paper 69-369 at the AIAA Hypervelocity Impact Conference, Cincinnati, Ohio, April 30–May 2, 1970; submitted April 29, 1970; revision received August 3, 1970. This research is supported by NASA Lewis Research Center, under Grant NGL-39-004-001.

* Professor of Aerospace Engineering. Associate Fellow AIAA.
† Research Associate. Member AIAA.

‡ Subscripts r and t affixed to ϕ and w designate partial differentiations.

Introduction

BUMPER-PROTECTED space structures, or double-walled structures, have been analyzed recently by many investigators. In all these studies a bumper is used to intercept the projectile. After the initial impact, the projectile and the bumper vaporize, or disintegrate, into a debris cloud, which then impacts on the main structure wall. The response of the main structure wall subject to this debris loading is studied in this paper.

In treating this problem, Madden,[1] McMillan,[2] Wilkinson,[3] and Thompson[4] all assumed that the loading of the debris is instantaneous, i.e., at time zero a certain amount of momentum and energy is deposited on the main structural wall. For times larger than zero the loading is supposed to be zero. This type of analysis may be satisfactory for long-time response of the structure; however, since it neglects the time history of the loading it cannot account for the early time (0 to 50μ-sec) response of the structure.

In the present analysis a detailed short-time response of the tank wall is considered. It is essentially an extension of the method used in Ref. 5 where the problem of particle impact on unprotected fuel tanks was studied. Since only short-time response is being considered, the shape and boundary conditions of the tank wall are not relevant; the wall may be treated as an "infinite" plate under axisymmetrical loading. Both sides of the plate are being loaded, the front side by the debris cloud, the back side by the reaction of the liquid fuel.

The pressure distribution in the debris cloud is approximated by an empirical formula. In presenting this formula, it is assumed that the pressure distribution is Gaussian, and is not affected by the wall motion. The loading due to reaction of the liquid fuel is calculated from the shock Hugoniot of the fuel and the velocity of the tank wall. Both the debris and fuel loadings appear as additional terms in the Uflyand-Mindlin plate equations. These equations are distinctly hyperbolic,[6] and the method of characteristics in finite difference form is used to solve them.

Calculated plate deflections are in agreement with experimental measurements. In the case of a water-filled tank, it is shown that the stresses and deflections are diminished by about one order of magnitude as compared with the corresponding case of an empty tank.

Debris Cloud Pressure on Main Wall

Among those who have made experimental measurements of the debris cloud are Becker, Watson, and Gibson[7]; Friend, Murphy, and Shanfield[8]; Lundberg, Stern, and Bristow[9]; and McMillan.[2] Becker et al. measured the spatial distribution of the mass of the debris cloud as a result of projectiles having velocities of up to 4 km/sec impacting on aluminum bumpers. Lundberg et al. measured the vertex angle of the spray cone for projectile impact at 15,000–25,000 fps on a variety of bumpers. Reference 8 reported the spatial distribution of pressure in the debris cloud incident upon an aluminum witness plate for Lexan on lead impacts at projectile velocities of up to 9 km/sec. McMillan photographed the debris cloud resulting from aluminum on aluminum impacts at projectile velocities of up to 8 km/sec in order to establish the area on the main plate on which the cloud pressure acts.

Due to the complexity of the governing equations, analytical study of the debris cloud has been limited to numerical calculation. Utilizing a two-dimensional particle in cell code, PICWICK, Riney and Heyda[10] calculated the spatial distribution of the forward axial momentum incident upon witness plates for aluminum on aluminum impacts at a projectile velocity of 7.6 km/sec. Rosenblatt, Kreyenhagen, and Romine[11] calculated the spatial distributions of debris cloud mass, axial momentum, and kinetic energy at witness plates for similar metal impacts at velocities up to 15 km/sec. A two-dimensional, hydrodynamic-elastic-plastic code, STEEP, was employed. In both these studies, all quantities presented show an approximately Gaussian spatial distribution.

Results from the aforementioned experimental and numerical studies of the debris are used by many investigators as guidelines in making simplified assumptions. These assumptions are necessary in specifying the debris load on the main wall in simple forms.

Madden[1] has assumed a Gaussian mass distribution in the debris cloud. In this theory no upper bound for the average cone spray angle is predicted. Wilkinson[3] has modified Madden's analysis to include a cutoff for the average cone angle which agrees more closely with experiment. In both these studies the standard deviation of the assumed Gaussian mass distribution is linearly proportional to the bumper to plate spacing S. Thompson[4] also assumed that the pressure impulse at the main wall is spatially Gaussian.

As mentioned before, in studying the motion of the main wall, the aforementioned investigators have all assumed that the debris delivers a certain amount of momentum instantaneously. For short-time response, we must consider the temporal variation of the debris loading as well as its spatial distribution. Guided by the existing experimental and numerical results, we devised the following empirical equation for the pressure loading on the main wall. It is

$$P(r,t) = P_1\left[\exp - \left(\frac{t - t_1}{t_o}\right)^2 - \exp - \left(\frac{t_1}{t_o}\right)^2\right] \times \exp - (r/\beta)^2, \quad 0 \leq t \leq 2t_1 \quad (1)$$

$$P(r,t) = 0 \qquad t > 2t_1$$

where t_1, t_o, P_1, and β are constants. This equation implies that the spatial pressure distribution is Gaussian. The constant β, which is proportional to the standard deviation factor, may be expressed as a linear function of the stand-off distance S between the bumper and the main wall.

For the example problems calculated here, the constants in Eq. (1) are determined by fitting the curve of Eq. (1) to the experimental data of Ref. 8. Figure 1 shows the experimental pressure distribution of the debris due to a 0.01-in.-thick lead bumper and a Lexan projectile traveling at 30,100 fps. Pressure probes were placed at $r = 0$, 2, and 4 in., all 6 in. downstream of the bumper. The constants P_1, t_o, and t_1 are determined to best fit the $r = 0$ curve. The constant β is selected to match the peak pressure at $r = 2$ in. The resulting error at $r = 4$ in. is considered not serious, since the magnitude of the pressure at this radius is rather small as compared with that at $r = 0$. For this example these constants are $P_1 = 30.013 \times 10^3$, $t_o = 4.30$; $t_1 = 12.0$, and $\beta = 1.65$.

Pressure Induced in the Liquid

The interaction between a moving plate and the adjacent liquid constitutes a two-space variable, unsteady, and coupled elastic-hydrodynamic problem. In order to render the analysis tractable, the motion of the liquid is considered to occur in the axial direction and the radial component of motion is neglected. In addition, the effects of viscosity are neglected.

A schematic diagram is shown in Fig. 2, where the motion of the plate and the fluid to the right of it is plotted in the z-t plane for a particular radial location $r = 0$. As the plate moves to the right, a family of right-traveling waves is created in the fluid. These are compression waves when the plate velocity increases, and rarefaction waves when the plate velocity decreases. No left-traveling waves will be excited unless either the right-traveling waves reach a solid boundary or shock waves are formed. For the numerical problems studied in this paper, we are interested in the motion of the plate for the first 30 μsec, a time period in which the maximum stress and deflection usually occur. As can be seen from the

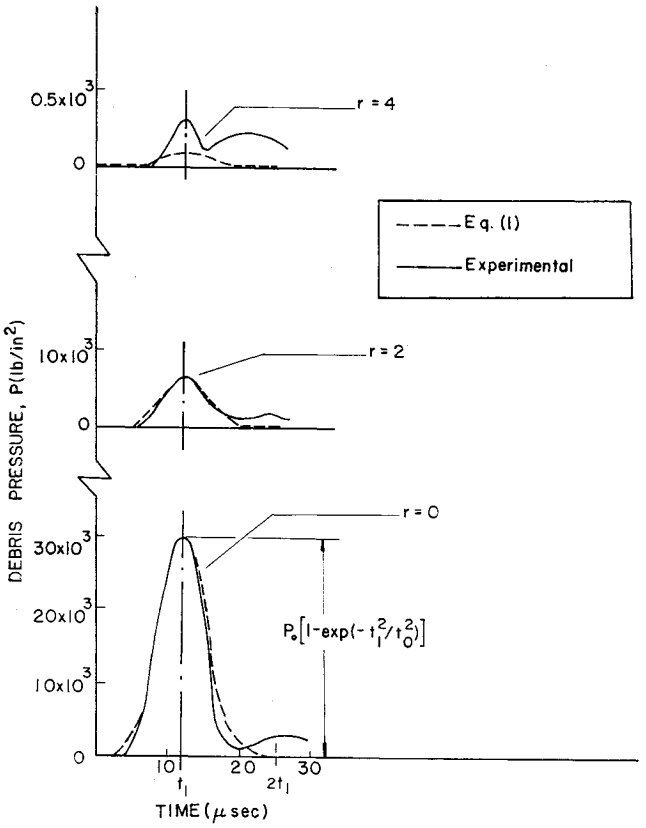

Fig. 1 Comparison of approximate and experimental debris pressure distributions; pressure vs time at several radii for a witness plate under debris loading from a 0.01-in. lead bumper 6 in. away, impacted by a 1.16 g Lexan projectile at 30,100 fps.

typical example in Fig. 2, the head of the compression wave has traveled a distance of only 18 in. in 30 μsec; and it is reasonable to assume that no solid boundary exists within this distance. The only source of left-traveling waves is the formation of a shock wave caused by the coalescence of right-traveling waves. This occurs at a time of 33 μsec after impact. For the present problem, we may therefore concentrate on the right-traveling wave during the first 30 μsec and ignore the left-traveling waves which occur later. In fact, the left-traveling waves caused by the shock do not influence the liquid at the plate surface until some time after 50 μsec.

In the absence of left-traveling waves, the fluid properties along each right-traveling wave are constant. To determine exactly the values of these properties, numerical integration across these waves would have to be performed.[12] This numerical integration process can be avoided if the change of properties across the right-traveling waves is approximated

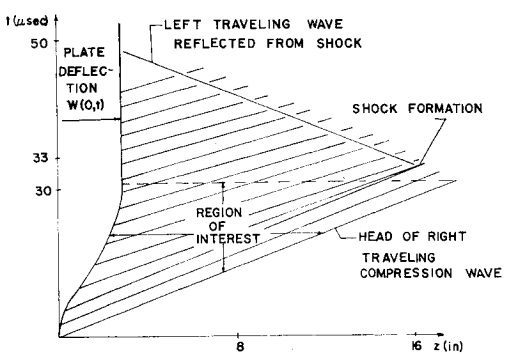

Fig. 2 Motion of the main plate and adjacent fluid in the z-t plane at a particular radial location, $r = 0$. The plate deflection curve w (0, t) is greatly exaggerated.

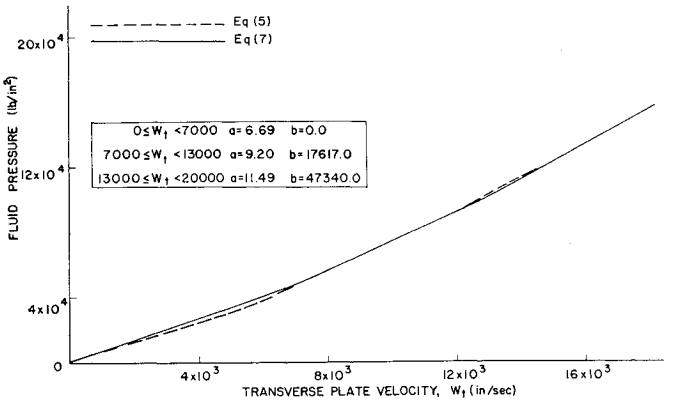

Fig. 3 Comparison of the exact and approximate water pressure behind the shock front; pressure vs transverse plate velocity.

by the shock relations. This approximation is known to be satisfactory if the wave is weak.[13] In the present problem, the maximum compression of the fluid is less than 7%, indicating that this method is acceptable.

The conservation equations across a shock are

$$u = (1 - \rho_o/\rho)U \tag{2}$$

$$P_f = P_o + (1 - \rho_o/\rho)\rho_o U^2 \tag{3}$$

In these equations the properties behind the shock are the density ρ, the pressure P_f, and the particle velocity u, and the shock velocity is denoted by U. The state ahead of the shock is described by the constants P_o and ρ_o, and the fluid is initially at rest. These two equations, combined with an empirical Hugoniot relation for water,[14]

$$U = 1.483 + 25.306 \log_{10}(1 + u/5.19) \tag{4}$$

where the velocities are in km/sec, constitute a system of three equations with four unknowns, ρ, u, P_f, and U. For small values of P_o, this system of equations reduces to

$$P_f = 3.6858u[1.483 + 10.99 \ln_e(1 + u/204330.1)] \tag{5}$$

where the pressure is given in psi and the particle velocity is given in in./sec. Since the particle velocity along each right-traveling characteristic is known, the pressure along the characteristic may be computed, giving the fluid load on the plate. The particle velocity of the fluid u is equal to the plate velocity $\partial w/\partial t$, or

$$u = \partial w/\partial t \tag{6}$$

where w is the transverse deflection of the plate.

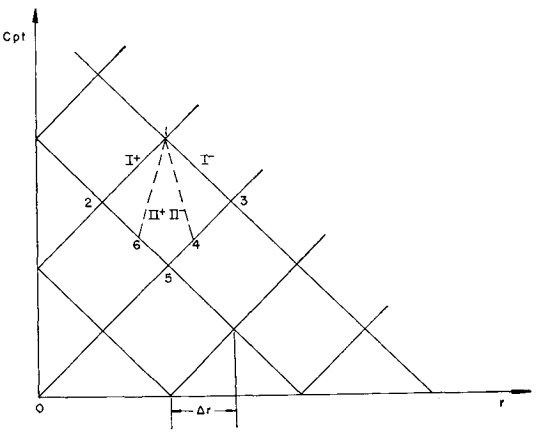

Fig. 4 Characteristic network for application of the numerical procedure.

For computational convenience the fluid pressure expression of Eq. (5) is approximated by three-line segments of the form

$$P_f(w_t) = a\partial w/\partial t + b \tag{7}$$

as shown in Fig. 3.

Stress Waves in Tank Walls

Governing Equations and Characteristic Relations

The Uflyand-Mindlin equations, in polar cylindrical coordinates, for a linearly elastic plate with normal surface tractions under the assumption of axisymmetric loading are the equilibrium equations

$$\partial M_r/\partial r + 1/r(M_r - M_\theta) - Q_r = (\rho_1 h^3/12)\partial^2\phi/\partial t^2 \tag{8}$$

$$\partial Q_r/\partial r + (1/r)Q_r + P(r,t) - P_f(w_t) = \rho_1 h(\partial^2 w/\partial t^2) \tag{9}$$

together with the plate constitutive relations

$$M_r = D(\partial\phi/\partial r + \nu/r\phi) \tag{10}$$

$$M\theta = D(\phi/r + \nu\partial\phi/\partial r) \tag{11}$$

$$Q_r = k_2^2 Gh(\phi + \partial w/\partial r) \tag{12}$$

Equations (8 and 10–12) are identical to Eqs. (10 and 12–14) of Ref. 5, and are reproduced here for convenience. Equation (9) differs from Eq. (11) of Ref. 5 by the addition of the debris load term $P(r,t)$ and the fluid contribution $P_f(w_t)$. Also, as in Ref. 5, the symmetry of the problem requires that $M_{r\theta} = Q_\theta = \partial/\partial\theta = 0$. The system of Eqs. (8–12) is hyperbolic and therefore amenable to the method of characteristics. Thus, following Ref. 5, we eliminate M_r, M_θ, and Q_r from Eq. (8) and Eq. (9) by Eqs. (10–12) to obtain the displacement equations of motion as

$$\frac{\partial^2\phi}{\partial r^2} - \frac{1}{c_p^2}\frac{\partial^2\phi}{\partial t^2} = \frac{k_2^2 Gh}{D}\left(\phi + \frac{\partial w}{\partial r}\right) + \frac{\phi}{r^2} - \frac{1}{r}\frac{\partial\phi}{\partial r} \tag{13}$$

$$\frac{\partial^2 w}{\partial r^2} - \frac{1}{k_2^2 c_2^2}\frac{\partial^2 w}{\partial t^2} = -\frac{1}{r}\left(\phi + \frac{\partial w}{\partial r}\right) - \frac{\partial\phi}{\partial r} - 1/k_2^2 Gh[P(r,t) - P_f(w_t)] \tag{14}$$

The characteristic directions of Eqs. (13) and (14) are

$$\left.\begin{matrix} I^+ \\ I^- \end{matrix}\right\} dr/dt = \pm c_p \tag{15}$$

$$\left.\begin{matrix} II^+ \\ II^- \end{matrix}\right\} dr/dt = \pm k_2 c_2 \tag{16}$$

Along the I^+ and I^- directions we have the compatibility equations (characteristic equations)

$$\frac{1}{c_p} d\phi_t \mp d\phi_r = \mp\left[\frac{k_2^2 Gh}{D}(\phi + w_r) + \frac{\phi}{r^2} - \frac{\phi_r}{r}\right]dr \tag{17}$$

where the upper signs refer to the I^+ direction, and the lower to the I^-. Similarly, along the II^+ and II^- directions we

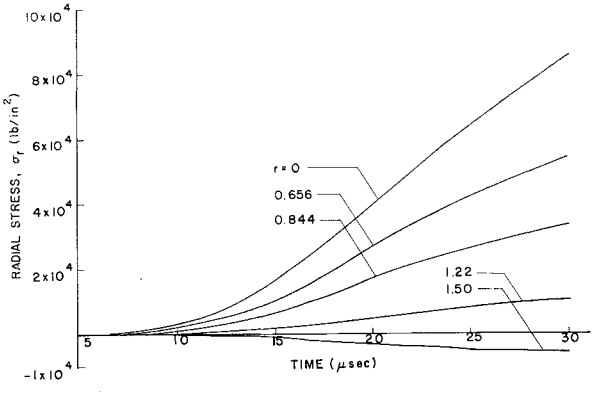

a) radial stress σ_r vs time

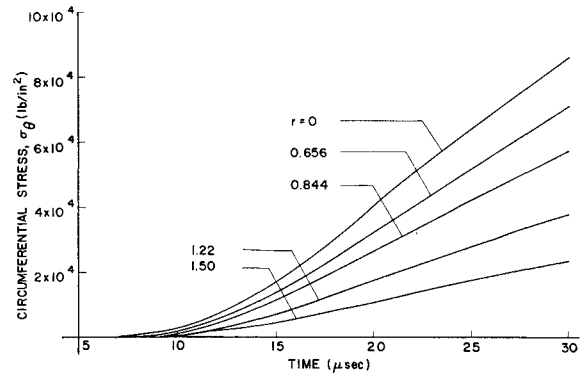

b) circumferential stress σ_θ vs time

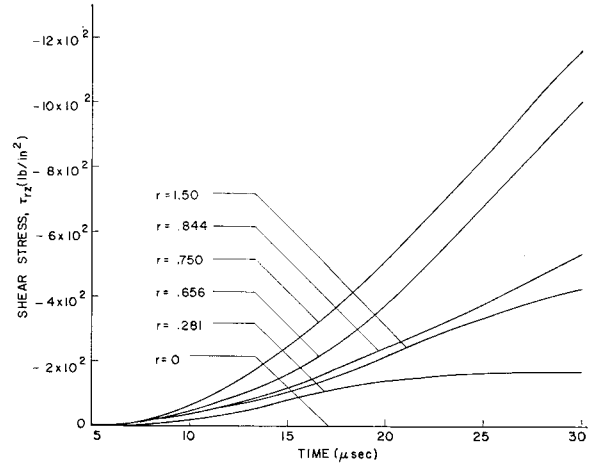

c) shear stress τ_{rz} vs time

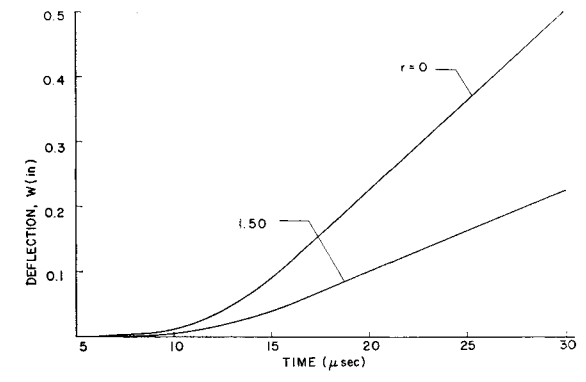

d) deflection w vs time

Fig. 5 Stress and deflection at several radii in an aluminum plate (no water backing, $h = \frac{1}{32}$ in.), with a 0.01-in. lead bumper 6 in. away, impacted by a 1.16 g Lexan projectile at 30,100/fps.

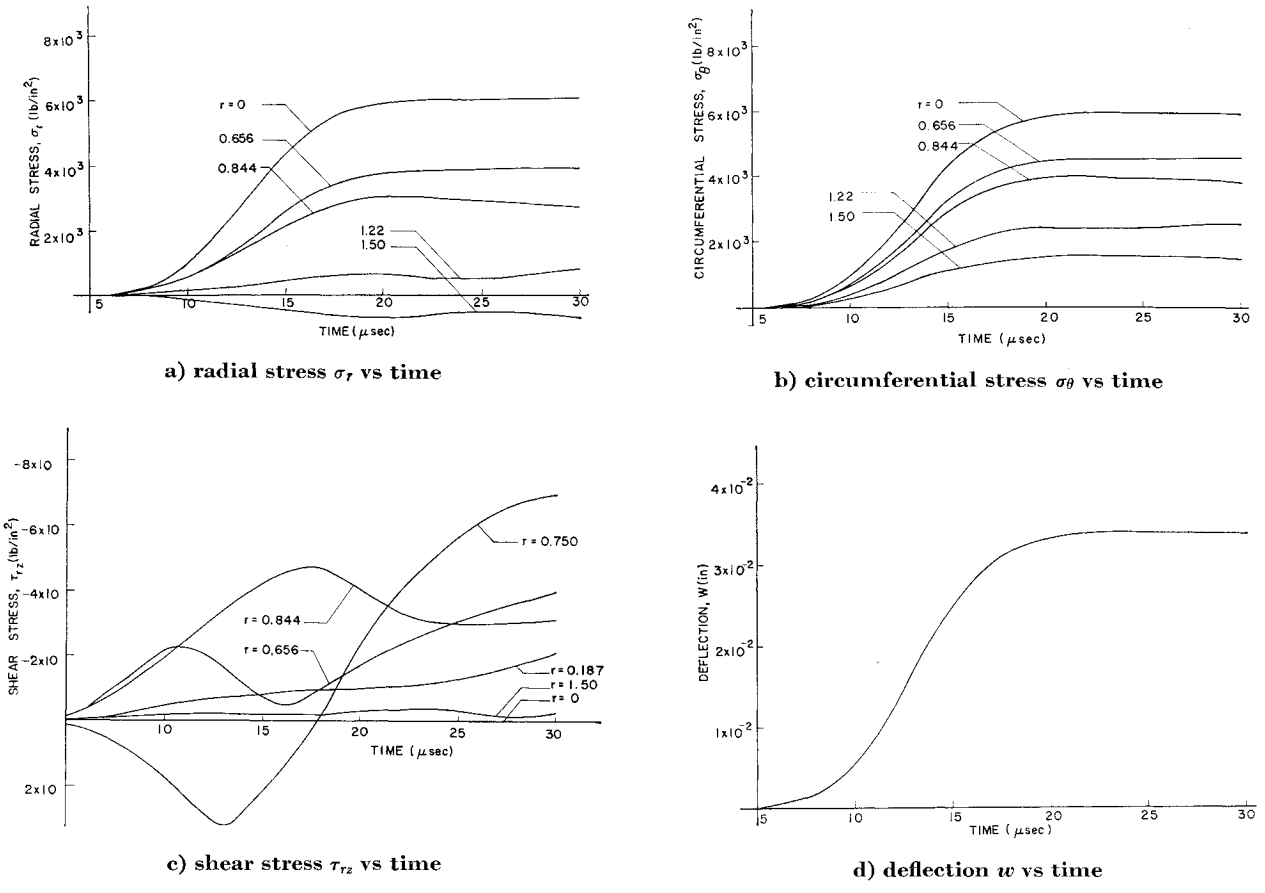

a) radial stress σ_r vs time

b) circumferential stress σ_θ vs time

c) shear stress τ_{rz} vs time

d) deflection w vs time

Fig. 6 Stress and deflection at several radii in an aluminum plate (water backed, $h = 1/32$ in.), with a 0.01-in. lead bumper 6 in. away, impacted by a 1.16 g Lexan projectile at 30,100 fps.

have

$$\mp \frac{1}{k_2 c_2} dw_t + dw_r = -\left[\frac{\phi}{r} + \frac{w_r}{r} + \phi_r + \frac{P(r,t)}{k_2^2 G h} - \frac{P_f(w_t)}{k_2^2 G h}\right] dr \quad (18)$$

Equations (17) and (18) are four equations in six unknowns: ϕ, ϕ_t, ϕ_r, w, w_t, and w_r. Two additional relations specifying the continuity of ϕ and w are

$$d\phi = \phi_t dt + \phi_r dr \quad (19)$$

$$dw = w_t dt + w_r dr \quad (20)$$

which are valid along any direction in the r, $c_p t$-plane where ϕ and w are continuous. Thus the Eqs. (17–20) form a system of six equations in six unknowns.

Exact Initial and Boundary Conditions

The problem considered in this paper is that of an infinite solid plate. Thus the region is specified by $0 \leq r < \infty$. Appropriate initial conditions for this problem require specification of ϕ_r, ϕ_t, w_r, and w_t at $t = 0$. For the present case where the plate is originally stationary, the initial conditions are

$$\phi(r,0) = \phi_t(r,0) = w(r,0) = w_t(r,0) = 0, \; 0 \leq r < \infty \quad (21)$$

At $r = 0$, a well-posed problem requires the specification of one of the following: w_r, w_t, M_r, or a linear combination of w_t and w_r. It also requires the specification of ϕ_r, ϕ_t, Q_r, or a combination of ϕ_t and ϕ_r. In the present impact situation the proper boundary conditions are

$$Q_r = \partial w/\partial r = 0 \text{ at } r = 0, \; 0 \leq t < \infty \quad (22)$$

which are consequences, respectively, of the loading and symmetry at $r = 0$.

Approximate Boundary Conditions

At $r = 0$ the cylindrical polar coordinate system is a singular point. Thus some of the terms in Eqs. (17) and (18) become indeterminate at $r = 0$. In the general finite difference scheme utilized here, special techniques would have to be introduced to handle such difficulties at $r = 0$.

In order to determine the value of $(1/r)w_r$ as $r \to 0$, the following technique is adopted. Let us assume the variable w_r and its derivatives are continuous along a constant time line $t = t_1$. Then w_r, at a point in the neighborhood of $r = 0$, $t = t_1$, may be expanded in a Taylor series about $r = 0$, $w_r(r,t_1) = w_r(0,t_1) + w_{rr}(0,t_1)r + w_{rrr}(0,t_1)r^2/2 + 0(r^3)$.

The first term in the right-hand side of the aforementioned equation vanishes. Thus, taking limit as r approaches zero yields

$$\lim_{r \to 0} \frac{w_r(r,t_1)}{r} = \lim_{r \to 0} \left\{w_{rr}(0,t_1) + w_{rrr}(0,t_1)\frac{r}{2} + 0(r^2)\right\} = w_{rr}(0,t_1) \quad (23)$$

From Eqs. (22) and (12), we have

$$\phi = 0 \text{ at } r = 0, \; 0 \leq t < \infty \quad (24)$$

Therefore the value of ϕ/r is indeterminate at $r = 0$. However, since the stress and acceleration must be finite at $r = 0$, the last two terms of Eq. (13) give

$$\phi/r = \phi_r \text{ at } r = 0, \; 0 \leq t < \infty \quad (25)$$

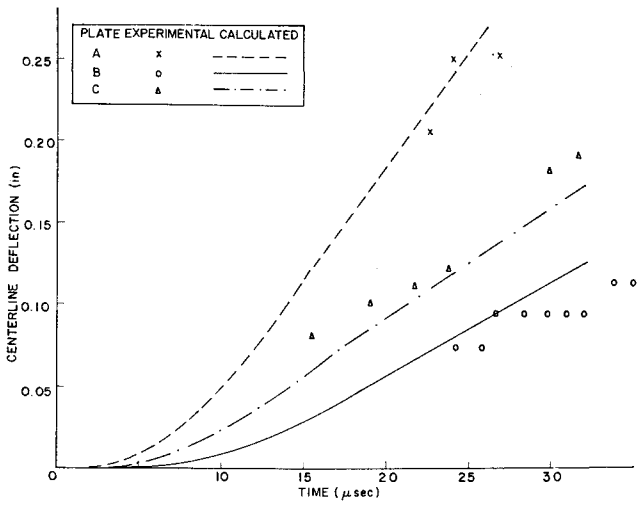

Fig. 7 Comparison of experimental and calculated centerline deflections of three aluminum plates (no water backing) with debris loadings as shown in Table 1.

By similar limiting process as in Eq. (23) the value of $1/r$ $(\phi/r - \phi_r)$ as $r \to 0$ can be obtained. The result is

$$\lim_{r\to 0} \frac{1}{r}\left[\frac{\phi(r,t_1)}{r} - \phi_r(r,t_1)\right] = -\phi_{rr}(0,t_1)/2 \qquad (26)$$

In the numerical computations, the values of $w_{rr}(0,t_1)$ and $\phi_{rr}(0,t_1)$ are approximated by the following expressions:

$$\phi_{rr}(0,t_1) = \frac{\phi_r(r,t_1) - \phi_r(0,t_1)}{r}, \quad w_{rr}(0,t_1) = \frac{w_r(r,t_1) - w_r(0,t_1)}{r} \qquad (27)$$

where r is the distance from $r = 0$ to the adjacent mesh point measured along $t = t_1$ line.

Numerical Procedures

Since the present problem differs from that of Ref. 5 only in the load terms and boundary conditions, the basic numerical scheme of Ref. 5 has been utilized. In the $c_p t$-r plane the I^+ and I^- characteristics intersect to form an orthogonal grid as shown in Fig. 4. Only at the intersection of the I^+ and I^- characteristics will properties be evaluated, despite the fact that there are four families of characteristics at every point of the plane. Consider now a typical interior point, or point 1 in Fig. 4. The line segments 1–4 and 1–6 lie along II^- and II^+, respectively. Values of the variables for point 4 are found by linear interpolation from points 3 and 5, while properties at point 6 rely on interpolation from points 5 and 2. Since three straight line segments are used for the fluid pressure P_f, a trial and error process is adopted to assure the proper straight line is used. The set of constants corresponding to one of the line segments is assumed for point 1. Given the values of all the dependent variables at points 2–6, we may write Eqs. (17–20) in finite difference form to provide six linear equations to solve for the six unknowns ϕ, ϕ_r, ϕ_t, w, w_r, w_t at point 1. If the calculated value of w_t does not fall on the assumed straight-line segment of Fig. 3, another segment must be chosen and the process repeated. Values of M_r, M_θ, and Q_r at point 1 may be constructed from the relations of Eqs. (10–12), respectively.

At points which lie along the boundary $r = 0$, the I^+ and II^+ characteristics are missing. In place of the compatibility equations along these two characteristics, the two boundary conditions, Eqs. (22) and (23), can be used. Thus, together with Eqs. (17), (18) (with the lower signs), (19), and (20), there are again six equations for the six dependent variables ϕ, ϕ_r, ϕ_t, w, w_r, and w_t.

Maximum Stresses

It may be shown that the components of stress σ_r, σ_θ, and τ_{rz}, according to the Uflyand-Mindlin plate theory are related to the bending moments and shear through[15]

$$\sigma_r = 12M_r z/h^3 \qquad \sigma_\theta = 12M_\theta z/h^3 \qquad (28)$$

$$\tau_{rz} = Q_r/k_2^2 h \qquad (29)$$

Thus the maximum normal stresses occur at $z = \pm h/2$ and have values

$$(\sigma_r)_{\max} = \pm 6M_r/h^2 \qquad (\sigma_\theta)_{\max} = 6M_\theta/h^2 \qquad (30)$$

while the maximum shear is given by Eq. (29).

Numerical Results and Comparison with Experiment

As numerical examples, the stresses and deflections in two identical plates, one without water backing and one with water backing, are calculated and presented. In all the examples given, a mesh size of 0.01875 in. is used for the numerical integrations. A mesh size of 0.009375 in. is also used for the example without water backing. The differences in magnitude for the stresses due to different mesh sizes are within 0.2%. The plate material is 7075-$T6$ Al having the following properties: $h = \frac{1}{32}$ in., $\rho = 0.2613 \times 10^{-3}$ lb-sec^2/in.^{4}, $G = 3.9 \times 10^6$ lb/in.^{2}, $k^2 = 0.85$, $E = 10.4 \times 10^6$ lb/in.^{2}, σ_y (static yield strength) $= 77 \times 10^3$ lb/in.^{2}, $\nu = \frac{1}{3}$. The debris loading is due to a Lexan pellet traveling at 30,100 fps impacting on a lead bumper.

Figures 5a–5d show σ_r, σ_θ, τ_{rz}, and w, respectively, as functions of time for several radii. These results are for a tank wall with no fluid behind. As can be seen, σ_r and σ_θ assume maximum values at $r = 0$, and as expected, they are equal at this location. The location where the maximum shear stress occurs is dependent on the spatial distribution of the loading. The total shear force is zero at $r = 0$ and increases as r increases. For the present case, the maximum shear stress occurs at $r = 0.75$ in. Comparing with σ_r and σ_θ, the shear stress τ_{rz} is much smaller. Up to a time of 30 μsec after impact, the deflection, σ_r and σ_θ at $r = 0$, and τ_{rz} at $r = 0.75$, are all still increasing with respect to time. Thus, it can be concluded that the stress governing the mode of (elastic) failure is the bending stress as expressed by Eq. (30), and the effects of shear are small.

The stresses and deflection of a fluid backed plate are presented in Figs. 6a–6d. The plate thickness and debris loading are exactly the same as the preceding case, except for the intro-

Table 1 Values of quantities involved in the three plate impact cases plotted in Fig. 7; plates are of 2024-$T3$ aluminum, bumpers are 0.01-in. lead, projectiles are 1.16 g Lexan

Cases	Bumper to plate spacing	Plate thickness	Projectile velocity	Debris pressure constants			
				P_1	t_o	t_1	β
A	6 in.	$\frac{1}{16}$ in.	26×10^3 fps	43.8×10^3	3.0	6.75	1.68
B	9 in.	$\frac{1}{16}$ in.	22×10^3 fps	10.5×10^3	5.5	10.0	2.17
C	6 in.	$\frac{1}{8}$ in.	26×10^3 fps	43.8×10^3	3.0	6.75	1.68

duction of the transverse fluid loading. As in the nonfluid backed case, the maximum normal stress occurs at $r = 0$. But the magnitude is about 14 times smaller. The deflection and the normal stresses reach their maximum values at 22 μsec, and maintain these values up to 30 μsec when our calculation terminates. The maximum shear stress still occurs at $r = 0.75$ in. for time larger than 26 μsec; at earlier times, τ_{rz} assumes opposite sign.

Limited experimental data are available from tests performed at Space Research Institute, Montreal, Canada. Figure 7 shows the comparison of experimental and calculated centerline deflection of three plates with no water backing under the debris loading given in Table 1. Agreement between our calculations and the test results is good.

Conclusions

Based on limited comparison with experimental evidence, we conclude the following:

1) The early time response of bumper-protected fuel-tank walls is adequately described by the present linear elastic analysis.

2) The maximum stress is that due to bending at the axis of symmetry. To predict the failure of the plate, an elastic-plastic analysis would have to be used.

3) The effects of a liquid backing are to reduce the deflection and maximum stress by approximately one order of magnitude over the unbacked case.

References

[1] Madden, R., "Ballistic Limit of Double-Walled Meteoroid Bumper Systems," TND-3916, 1967, pp. 8–10, NASA.

[2] McMillan, A. R., "Final Report on Experimental Investigations of Simulated Meteoroid Damage to Various Spacecraft Structures," TR 66-67, NASA CR-915, 1966, General Motors Defense Research Lab., Santa Barbara, Calif., p. 34.

[3] Wilkinson, J. D., "A Penetration Criterion for Double-Walled Structures Subject to Meteoroid Impact," *AIAA Journal*, Vol. 7, No. 10, Oct. 1969, pp. 1937–1943.

[4] Thompson, R. G., "Plastic Behavior of Circular Plates Under Transverse Impulse Loadings of Gaussian Distribution," TR R-29, 1968, NASA, p. 1.

[5] Chou, P. C., Schaller, R., and Hoburg, J., "Analytical Study of the Fracture of Liquid-Filled Tanks Impacted by Hypervelocity Particles," Rept. 160-9, NASA GR-72169, March, 1967, Drexel Institute of Technology, Philadelphia, Pa.

[6] Chou, P. C. and Perry, R. F., "The Classification of Partial Differential Equations in Structural Dynamics," *Proceedings of the AIAA Structural Dynamics and Aeroelasticity Specialist Conference*, New Orleans, La., April 16–17, 1969, pp. 185–194.

[7] Becker, K. R., Watson, R. W., and Gibson, F. C., "Hypervelocity Impact Phenomena," Quarterly Rept., BRL Authorization No. 4086, April 5, 1962, Bureau of Mines, U.S. Department of Interior.

[8] Friend, W. H., Murphy, C. L., and Shanfield, I., "Review of Meteoroid-Bumper Interaction Studies at McGill University," S.R.I.-R-15, NASA CR-54857, Aug. 1966, Space Research Institute, Montreal, Canada.

[9] Lundberg, J. F., Stern, P. H., and Bristow, P. H., "Meteoroid Protection for Spacecraft Structures," Aerospace Group, D2-24056, NASA CR-54201, Oct. 1965, Boeing Company, Seattle, Wash.

[10] Riney, T. D. and Heyda, F. J., "Theoretical Calculations for Meteor Bumper Systems," *Proceedings of the AIAA Symposium on Structural Dynamics and Aeroelasticity*, AIAA, New York, 1965, pp. 406–418.

[11] Rosenblatt, M., Kreyenhagen, K. N., and Romine, W. D., "Analytical Study of Debris Clouds Formed by Hypervelocity Impacts on Thin Plates," AFML-TR-68-266, Dec. 1968, Shock Hydrodynamics, Inc., Sherman Oaks, Calif.

[12] Chou, P. C. and Burns, B. P., "Late Stage Equivalence in One-Dimensional Impacts," *Journal of Applied Physics*, Vol. 38, No. 2, Feb. 1967, pp. 553–560.

[13] Shapiro, A. H., *The Dynamics and Thermodynamics of Compressible Fluid Flow*, Vol. II, Chap. 25, Roland Press Co., New York, 1954.

[14] Rice, M. H. and Walsh, J. H., "Equation of State of Water to 250 Kilbars," *Journal of Chemical Physics*, Vol. 26, 1967, p. 834.

[15] Mindlin, R. D., "Influence of Rotary Inertia and Shear on Flexural Motions of Isotropic, Elastic Plates," *Transactions of the ASME; Journal of Applied Mechanics*, March 1951, pp. 31–38.